Reconstruction of sedimentation changes under anthropogenic influence in a medium-scale estuary based on a decadal chronological framework

Zhixin Cheng, Xiao Hua Wang, Isabel Jalón-Rojas, Yue Liu

Reconstruction of sedimentation changes under anthropogenic influence in a medium-scale estuary based on a decadal chronological framework

Cheng, Z., Wang, X.H., Jalón-Rojas, I., Liu, Y.

DOI

10.1016/j.ecss.2019.106295

Publication date

2019

Document version

Accepted author manuscript

Published in

Estuarine, Coastal and Shelf Science

Citation

Cheng, Z., Wang, X.H., Jalón-Rojas, I., Liu, Y. (2019) Reconstruction of sedimentation changes under anthropogenic influence in a medium-scale estuary based on a decadal chronological framework, Estuar. Coast. Shelf Sci., in press. doi:10.1016/j.ecss.2019.106295.

Accepted Manuscript

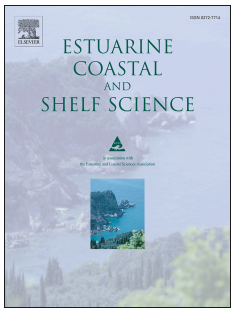

Reconstruction of sedimentation changes under anthropogenic influence in a medium-scale estuary based on a decadal chronological framework

Zhixin Cheng, Xiao Hua Wang, Isabel Jalon Rojas, Yue Liu

PII: S0272-7714(18)30999-5

DOI: https://doi.org/10.1016/j.ecss.2019.106295

Article Number: 106295

Reference: YECSS 106295

To appear in: *Estuarine, Coastal and Shelf Science*

Received Date: 30 November 2018

Revised Date: 7 July 2019

Accepted Date: 17 July 2019

Please cite this article as: Cheng, Z., Wang, X.H., Rojas, I.J., Liu, Y., Reconstruction of sedimentation changes under anthropogenic influence in a medium-scale estuary based on a decadal chronological framework, *Estuarine, Coastal and Shelf Science* (2019), doi: https://doi.org/10.1016/j.ecss.2019.106295.

Reconstruction of sedimentation changes under anthropogenic influence in a medium-scale estuary based on a decadal chronological framework

Zhixin Cheng [a,b,*], Xiao Hua Wang [a,b], Isabel Jalon Rojas [a,b] and Yue Liu [c]

a The Sino-Australian Research Centre for Coastal Management, University of New South Wales, P.O. Box 7916, Canberra, BC 2610, ACT 2600, Australia

b School of Science, University of New South Wales, P.O. Box 7916, Canberra, BC 2610, ACT 2600, Australia

c Urban Construction College, Eastern Liaoning University, Dandong 118003, China

***** Correspondence:

E-mail address: Zhixin.Cheng@student.adfa.edu.au;
Tel.: +61-45-6308-574

ABSTRACT

The present study uses sedimentary records from the Yalu River Estuary (YRE) over the past five decades to establish a regional age framework and investigate the influence of anthropogenic activity. Ten sediment core samples collected from various locations in the estuary were analysed. Core-averaged sediment accumulation rates calculated based on the ^{210}Pb and ^{137}Cs profiles of these samples were in the range 1.09–2.83 and 0.94–3.11, respectively. A regional age framework with major environmental events was established assuming the deposition rate in a section was constant. The age framework showed that most of the sediments in the YRE were deposited from the 1960s, and a grain size analysis also evidenced that the sedimentary environment experienced dramatic change after 1963. Changes in sedimentary environment in the estuary due to human activity (e.g. dam construction, deforestation and large mining activities) were also discussed: (1) the mean grain size at sites near the main channel became finer after 1963 due to the contemporaneous reduction in sediment discharge caused by upstream reservoir construction; (2) abnormal ^{137}Cs signals in the records during the 1980s probably reflected a concurrent deforestation, and the ^{137}Cs signals in the 1990s were related to mixing of sediments caused by mining activities. Results of this study demonstrate that sedimentation processes in a medium-scale estuary can be greatly changed under anthropogenic influence. The feasibility of using ^{137}Cs time markers (especially auxiliary time markers in 1975 and 1986) in a dynamic estuary is confirmed in this study. Furthermore, the regional age framework established in this study can provide a chronological reference for future studies in the YRE and adjacent areas.

Keywords: ^{210}*Pb;* ^{137}*Cs; sediment accumulation rate; age framework; anthropogenic influence; sedimentary event*

1. Introduction

Sedimentation processes in estuaries and coastal areas contain information related to morphology evolution, the characteristics of the eco-environment and materials exchange with adjacent aquatic systems. Decadal and longer-timescale sediment studies can address the issue of how the sedimentary environment responds to human activities (Wang et al., 2016). Thus, it is of great value to investigate the historical changes in sedimentation in medium-scale estuaries which are sensitive to anthropogenic processes. Long-term continuous monitoring data of sediments are unavailable for many regions; interpretation of sedimentary records in core samples is an alternative approach to obtain past sedimentation characteristics in estuaries. In order to reconstruct the sedimentation history, dating of these records is essential; an age framework is the cornerstone for further elemental analysis of major elements, trace elements, organic matter, rare-earth elements and heavy metals.

A widely accepted dating method for marine sediments uses lead-210 (^{210}Pb) profiles (Abril, 2016; Kirchner, 2011; Ruiz-Fernández and Hillaire-Marcel, 2009). The radionuclide ^{210}Pb was first applied to marine-sediment chronology on the Californian coast by Koide (1972) and, since then has been commonly used for oceans, lakes, gulfs, and estuaries around the world (Martins et al., 2012; Mulsow et al., 2009; Prajith et al., 2016; Simms et al., 2008). Sedimentary records in coastal areas are often discontinuous or have low activity ^{210}Pb due to

disturbance from floods, storm surges and human activity. The regular exponential-decay curves for ^{210}Pb dating are not present in these areas (Humphries et al., 2010; Jia et al., 2018; Kirchner, 2011). Although continuous decay curves may be absent for coastal sediment samples, ^{210}Pb sections with relatively clear exponential decay can be used for estimating sediment accumulation rates (Gwiazda et al., 2015; Li and Gao, 2012; Qiao et al., 2017).

Previous studies have suggested that other independent time markers such as cesium-137 (^{137}Cs) should be used together with ^{210}Pb for greater accuracy (Humphries et al., 2010; Kirchner, 2011). The artificial radionuclide ^{137}Cs was created during the nuclear explosions of 1945, and was first detected from sediments in 1954 (Ritchie and McHenry, 1990). Both the USA and the Soviet Union performed numerous nuclear tests before the establishment of the Partial Test Ban Treaty in 1963. As a consequence, the largest accumulation of ^{137}Cs activity found in Northern Hemisphere sediments generally corresponded to the year 1963, later becoming an important and widely used sediment time marker (Leroy et al., 2013; Simms et al., 2008). Similarly, nuclear tests performed by several developing countries in the early 1970s resulted in the 1975 ^{137}Cs time marker (Jha et al., 2003). Later on, the Chernobyl nuclear power station accident in 1986 produced the third time marker (Tsabaris et al., 2015; Varley et al., 2017). These two auxiliary ^{137}Cs time markers, in 1975 and 1986, have also been widely adopted in previous studies (Andersen et al., 2000; Ligero et al., 2005; Tsabaris et al., 2015). Some studies proposed the possibility of the existence of a fifth ^{137}Cs fallout following the 2011 Fukushima nuclear accident (Kato et al., 2012; Tsurumura et al., 2013). Those important ^{137}Cs time markers corresponding to the

contemporaneous ^{137}Cs deposition peaks in sedimentary records can be used as dating references for recent marine sediments. In addition to the application in sediment dating, distinct ^{137}Cs and ^{210}Pb signals in the sediment cores contain retrospective information about sedimentation changes caused by natural or anthropogenic processes (Gao et al., 2017; Humphries et al., 2010).

The Yalu River is the northern-most point of the coastline of China and is located at the junction of three economic zones: the Northeastern Asian Economic Rim; the Bohai Sea Rim; and the Yellow Sea Economic Rim. Numerous activities, including harbour and reservoir construction, dredging, mining and land reclamation have been conducted in the Yalu River Estuary (YRE) and adjacent Northern Yellow Sea (NYS) area. These human activities have changed the estuarine morphology and hydrodynamics in the YRE (Gao et al., 2012; Shi et al., 2017). The Yalu River also forms part of the border between China and North Korea; a previous study showed that the China has experienced severe land loss because erosion of the west bank of the river (in China) is stronger than on the east. As a consequence, the borderline moved westward from 1976 to 2010 (Li et al., 2012). Accordingly, it is crucial to understand sedimentary records from this region to improve coastal management and address this borderline-change issue (land loss of China). Moreover, taking YRE as a case study for sedimentary records can facilitate a more comprehensive understanding of the anthropogenic influence on estuarine process in a medium-scale estuary. Sedimentation processes in the YRE are also of significance in studying material exchange and transport in the Yellow Sea (Shi et al., 2018). Previous sediment studies in the YRE used surficial sediment samples or

limited numbers of core samples from the western estuary (Gao et al., 2009; Li et al., 2014; Liu et al., 2017, 2013; Shi et al., 2017). The sedimentation processes in the Main Branch and the vertical distribution of ^{137}Cs in the YRE remain unrevealed.

This study aims to establish an age framework for sedimentary records in the YRE based on ten sediment core samples collected from the Main Branch in 2014. External events reflected by the changes in sedimentation rates in the estuary were also analysed. Furthermore, we investigated the historical variation in particle grain size and ^{137}Cs level under anthropogenic influence.

2. Materials and methods

2.1 Study area

The Yalu River is the largest river flowing into the NYS, with annual runoff and sediment discharge of 2.67×10^{10} m^3 and 1.59×10^{6} t, respectively (Cheng et al., 2016). There are three main water outlets of the Yalu River (Fig. 1). The West River runs to the west of Chouduan Island, the main water outlet, the East Branch, runs to the east of Chouduan Island and is further divided into the Middle River and East River. To the south is the Split Flat between the Middle River and East River, and the prodelta, both of which are submerged at high tide and exposed (and joined) at low tide.

The hydrodynamics in the study area is controlled by the interaction of tides, river flow and wave action. The YRE is dominated by regular semi-diurnal tides with an average tidal range of 4.6 m and a maximum tidal range of 6.7 m; the tidal currents can be up to 2 m/s

(Cheng et al., 2016). There is an asymmetry in tidal duration in the YRE, with longer ebb period than flood. Wave action in this area is relatively weak, with the average significant wave height outside the estuary of 0.5 m (Yu et al., 2014). According to monitoring data from the Donggang Tide Gauge Station, the significant wave height can occasionally reach up to 2.4 m, which has happened five times during the last ten years.

There is a turbidity-maxima area in the YRE that covers a 10–20 km stretch located between 30 km and 60 km from the upstream tidal limit (Gao et al., 2004; Yu et al., 2014). Tidal pumping has been proposed as the dominant mechanism for turbidity maxima formation (Yu et al., 2014).

2.2 Sample collection and data pre-treatment

Sample collection

Ten sediment cores (K1, K2, K4, K5, K6, K8, K9, K10, K11 and K12 in Fig. 1) were collected in August 2014 from different areas around the YRE in this study. These cores were sampled by inserting a PVC tube with an inner diameter of 85 mm and an outer diameter of 90 mm into the sea-bed surface during low slack water, with the water level less than 1 m. The samples were then divided into 2cm-thick sub-samples and sent to the laboratory for radioactive-element detecting and grain size analysis. In addition to these ten sediment cores from the present study, results from four other sediment cores (C2, C3, C4 and C5) collected in 2013 by Liu et al. (2017), using the same sampling and data processing method, were also analysed for long-term change of grain size and vertical variation of ^{137}Cs. We note that these

144 analyses have not been discussed in Liu et al. (2017).

145 ***Grain size analysis***

146 A laser particle-size analyzer, BT-9300HT, was used to measure the sediment grain
147 size of the samples. The sub-samples were first put into water which had been sitting for 24
148 hours, then 10–20 ml of dispersant made of $(NaPO_3)_6$ at a concentration of 0.05 mol/L were
149 added. Determination of particle grain size was conducted using the Collias equal-moment
150 formula (Collias, 1943). Grain size parameters (skewness, kurtosis and sorting coefficient)
151 were calculated according to Folk and Ward (1957).

152 ***Radioactivity measurements***

153 The ^{210}Pb and ^{137}Cs radioactivity measurements were conducted in the State Key
154 Laboratory of Lake Science and Environment, Nanjing Institute of Geography & Limnology,
155 Chinese Academy of Sciences. Data were collected using a γ spectrum analyzing system from
156 EG&G ORTEC. The detector was placed in a lead chamber with a wall consisting of three
157 layers: a 5mm-thick organic glass layer; a 3mm-thick copper layer; and a 2mm-thick lead
158 layer. The ^{137}Cs and ^{226}Ra reference standard samples were provided by the China Institute of
159 Atomic Energy, the ^{210}Pb reference standard samples by the University of Liverpool.

160 ^{226}Ra activity was first measured to obtain the background value of ^{210}Pb (the supported
161 ^{210}Pb), then the supported ^{210}Pb value was removed from the measured total ^{210}Pb activity to
162 obtain the excess activity of the ^{210}Pb ($^{210}Pb_{ex}$). Then the $^{210}Pb_{ex}$-based sediment accumulation
163 rates were calculated using the Constant Initial Concentration (CIC) mode (Appleby, 1997;

Szmytkiewicz and Zalewska, 2014). This method assumes that the ^{210}Pb activity when it is deposited at the sediment-water interface is constant, which is reasonable for systems dominated by erosional input (Kumar et al., 2016). The ^{210}Pb activity at any depth using the CIC mode can be expressed as:

$$C_{\square} = C_0 e^{-\lambda t} \quad (1)$$

where $C_{\square}$ (Bq/kg) is the activity of ^{210}Pb at depth $\square$ in the core, C_0 (Bq/kg) the measured activity at depth 0, λ the decay constant of ^{210}Pb, 0.0314/yr, and t (yr) is the age of the sediment layer at core depth $\square$.

For the ^{137}Cs analysis, the sedimentation rate of ^{137}Cs was calculated based on the ^{137}Cs maximum layer, which corresponds to the key time marker of 1963. The age of other layers was obtained based on the sedimentation rate of the known marker. Although there might be an upward or downward diffusion of the ^{137}Cs peaks, it would not change the position of the ^{137}Cs peaks in the sedimentary profiles or affect the use of the ^{137}Cs peak time markers (Zapata, 2002; Zhang *et al*., 2012). The ^{137}Cs-derived sedimentation rate for a sample was calculated using following equation:

$$r = H/(n - 1963) \quad (2)$$

where r is the sedimentation rate (cm/yr) for this sample, H the depth (cm) of the ^{137}Cs peak for the 1963 time marker, and n the year of sampling. Thus, the age for the layers deposited above the 1963 time marker depth can be expressed as:

$$T_n = 1963 + (H - h_n)/r \quad (3)$$

where T_n and $\square_n$ are the age (yr) and depth (cm) for this layer, respectively. For the layers

185 deposited below the 1963 time marker depth, the age was calculated as follows:

186 $$T_0 = 1963 - (h_0 - H)r \quad (4)$$

187 where T_0 and h_0 are the age (yr) and depth (cm) for this layer, respectively.

188 ***Estimation of the ^{137}Cs atmospheric deposition flux in the YRE***

189 The atmospheric deposition flux of ^{137}Cs can be estimated based on an established
190 algorithm using precipitation data and the ^{137}Cs concentration in rain water (Pálsson et al.,
191 2006):

192 $$D_{xi} = C_{ri}P_{xi} \quad (5)$$

193 where D_{xi} is the ^{137}Cs atmospheric deposition flux and P_{xi} the precipitation (mm) at site x
194 during time period i. C_{ri} is the ^{137}Cs concentration in the precipitation at the reference site r
195 during the same time period (Bq·m^{-3}).

196 The redistribution of ^{137}Cs in the atmosphere is mainly controlled by wind, so that ^{137}Cs
197 deposition in a specific region depends on the latitude and on the amount of local
198 precipitation (Poręba and Bluszcz, 2007; Ritchie and McHenry, 1990). There is no record of
199 ^{137}Cs fallout in the YRE region, thus, it was estimated using the monitoring data in Tokyo
200 (which is located in the same latitudinal wind zone as the YRE) using the equation:

201 $$D_{YR} = D_{TK}P_{YR}/P_{TK} \quad (6)$$

202 where D_{YR} (Bq·m^{-2}/yr) and D_{TK} (Bq·m^{-2}/yr) are the ^{137}Cs atmospheric deposition flux in
203 the YRE and Tokyo for year i, respectively. P_{YR} and P_{TK} are the annual precipitation
204 amount in the YRE and Tokyo for year i, respectively.

205 The ideal annual ^{137}Cs atmospheric deposition curve for the YRE region from 1951 to

2008 was calculated based on Eq. (6) using precipitation data from the Dandong Meteorology Station and the annual ^{137}Cs atmospheric deposition flux and precipitation rate of Tokyo (Japan Meteorological Agency, 2001).

3. Results

3.1 Sedimentation rate for sedimentary records in the YRE

The dating results and vertical profiles of ^{210}Pb and ^{137}Cs for the ten collected cores in this study are shown in Fig. 2. The ^{210}Pb decay curves were classified into five types based on their patterns: two-section curves (the decay and background sections); three-section curves (the disturbance, decay and background sections); and multi-section curves (two-decay, disordered and inverted curves), disordered curve and inverted curve. According to the number of ^{137}Cs peaks, the vertical ^{137}Cs profiles were classified into four types: multiplet; triplet; doublet and singlet.

Cores K1, K2, K4, K8, K9, K10 and K12 contained one continuous ^{210}Pb decay section which was used to calculate the ^{210}Pb-based sedimentation rate for these cores. Core K5 had two ^{210}Pb decay sections; deposition ages in this core were determined according to the sectional sedimentation rate. For K6 and K11, the ^{210}Pb-based sedimentation rate could not be derived due to the abnormal exponential decay. The range of the core-averaged ^{210}Pb-based sedimentation rates for the ten samples was 1.09–2.83 (Table 1 and Fig. 3).

The ^{137}Cs-based sedimentation rates were determined according to the 1963 key time marker. The largest ^{137}Cs peaks in the vertical profiles were identified as the 1963 key time

226 marker except in K9, K11 and K12 (Fig. 2). For K9, K11 and K12, the second-highest peak
227 was considered the 1963 key time marker (Fig. 2). The identification of these time markers in
228 the YRE is discussed in Section 3.2. The range of the core-averaged ^{137}Cs-based
229 sedimentation rates using the 1963 key time marker was 0.94–3.11 (Table 1 and Fig. 3),
230 agrees well with the ^{210}Pb-based sedimentation rates.

231 Both the core-averaged ^{210}Pb-based and ^{137}Cs-based sedimentation rates in the cores
232 from the Split Flat (K10, K11 and K12) and prodelta (K1, K2, K8 and K9) were generally
233 larger than those from the River Island (K4, K5 and K6) (Table 1). Although the
234 sedimentation rate showed a slightly seaward-increasing trend, the spatial variation in the
235 sedimentation rate in these ten cores was relatively small, with standard deviations of 0.55
236 and 0.52 for the core-averaged ^{210}Pb-based and ^{137}Cs-based sedimentation rates, respectively.

237 *3.2 Time markers of ^{137}Cs in the YRE and the establishment of a*
238 *chronological framework*

239 As introduced in Section 1, previous studies proposed four major ^{137}Cs peaks in
240 deposition profiles, which roughly correspond to years when nuclear activities were
241 conducted globally. The corresponding dates of these ^{137}Cs peaks are termed “time markers”,
242 which represent the approximate time when the related sediment layer was deposited.
243 However, there could be uncertainty in the application of several time markers in different
244 locations due to the different regional atmospheric ^{137}Cs deposition fluxes. Figure 4 shows
245 the annual atmospheric ^{137}Cs deposition flux in the YRE region calculated from Eq. (6). The

246 total amount of ^{137}Cs fallout reached high levels during 1954, 1958 and 1963, followed by
247 lower levels in 1970, 1975 and 1986. The ^{137}Cs peaks in marine sediment cores
248 corresponding to the fallout peaks in 1954, 1963, 1975 and 1986 were identified in the cores
249 collected for this study. Although there were large ^{137}Cs atmospheric depositions in 1958 and
250 1970, they were not recognized as time markers in the marine sediment records as they were
251 close to the ^{137}Cs peaks in 1963 and 1975. The identification of the four important ^{137}Cs time
252 markers in the ^{137}Cs profiles is discussed in the following section.

253 *3.2.1 1963 Key Time Marker for ^{137}Cs*

254 The largest ^{137}Cs peaks in seven of the ten collected cores in this study corresponded to
255 1963 (Fig. 2), suggesting that the ^{137}Cs peak of 1963 was common and could be a useful time
256 marker for the YRE sediments. The deposition ages of the ^{137}Cs maximum layer in these
257 seven cores were verified by the ^{210}Pb dating method: differences in the sedimentation rates
258 between the two methods were small (Figs. 2 and 3) in all samples except for K6, for which
259 no ^{210}Pb-based sedimentation rate was available for comparison. Therefore, these ^{137}Cs peaks
260 can be considered as reliable 1963 time markers. In other three cores (K9, K11 and K12), the
261 maximum ^{137}Cs concentrations did not correspond to 1963. For core K11, an extremely high
262 ^{137}Cs level was found at the 36 cm layer, corresponding to 1992, while the ^{137}Cs levels in the
263 layers above and below were all less than detectable limit (Fig. 3). The reason for this peak is
264 discussed later in Section 4.2.2. The second highest ^{137}Cs peak in K11 was considered to be
265 the 1963 time marker. The ^{137}Cs-based sedimentation rates in cores K9 and K12 using the
266 largest ^{137}Cs peaks were evidently different from the ^{210}Pb-based results. However, by using

the second highest ^{137}Cs peaks, the ^{137}Cs-based sedimentation rates in these two cores matched the results calculated based on ^{210}Pb (Table 1). Therefore, the second highest ^{137}Cs peaks in K9 and K12 were considered to be the 1963 ^{137}Cs key time markers (the reason for the largest ^{137}Cs peaks in these two cores is discussed in Section 4.2). Similar results have been reported from other environmental settings (Li and Gao, 2012; Ruiz-Fernández et al., 2005; Wang et al., 2014).

3.2.2 1954 Auxiliary Time Marker for ^{137}Cs

The 1954 auxiliary time marker corresponds roughly to a ^{137}Cs peak accumulated after the nuclear explosions of 1945 (Gwiazda et al., 2015); it was identified here in cores K4 and K10 (Fig. 2). The ^{137}Cs peak at depth 76 cm in core K4 was dated to 1944 from a ^{210}Pb decay section and the 1963 ^{137}Cs time marker. Given that the ^{137}Cs was first produced in the 1950s, the ^{137}Cs peak here was corrected to be the 1954 time marker. The ^{137}Cs peak at 172 cm in K10 was dated to 1955 using the 1963 ^{137}Cs time marker for this core. The dating results for K10 based on the ^{210}Pb levels below 60 cm showed similar results. Therefore, it can be concluded that the ^{137}Cs peak at 172 cm in this core represented the 1954 time marker.

3.2.3 1975 and 1986 Auxiliary Time Markers for ^{137}Cs

In the ^{137}Cs sedimentary records from the YRE, five ^{137}Cs peaks (in K1, K2, K4, K5 and K10) were found corresponded to years around 1975 or 1986 (Table 1 and Fig. 2).

The 1975 auxiliary time marker (indicators for nuclear tests in 1970s) was identified in cores K2 and K4: the peak in ^{137}Cs concentration at 80 cm in K2 was dated to 1972 and that

287 at 38 cm in K4 to 1974 using the ^{210}Pb decay curve combined with the 1963 ^{137}Cs time
288 marker, both close to the year 1975. Considering the sedimentation rates based on the 1963
289 key time marker agreed well with those calculated from the ^{210}Pb decay section, it is
290 suggested that the 1975 time markers can be recognized in K2 and K4.

291 The 1986 auxiliary time marker was found in cores K1, K2 and K5: the ^{137}Cs peaks at
292 40 cm in core K1 (dated to 1989), 62 cm in core K2 (dated to 1982) and 34 cm in core K5
293 (dated to 1988) can be considered as 1986 time markers. Therefore, the ^{137}Cs peaks indicate
294 the 1975 and 1986 ^{137}Cs time markers can be adopted in the YRE although it can only be
295 tracked in several samples. However, the 1986 time marker should be applied with caution
296 due to the deposition hiatus in cores K1, K2, and K5.

297 More than 70% of the ^{137}Cs peaks in these profiles were time markers, which confirmed
298 that ^{137}Cs is feasible to be an independent time marker for sediment dating in the YRE. Based
299 on the analysis of ^{137}Cs time markers and ^{210}Pb dating results in the YRE, K4 and K10 can be
300 used as standard vertical profiles in the YRE and NYS to establish an age framework,
301 together with cores K2, K5, K6, and K11 as auxiliary profiles (Fig. 5).

302 *3.3 Lithological characteristics and grain size*

303 The sectioned lithological features of the YRE cores are shown in Fig. 6. Most
304 sediments from cores near River Island (K4, K5 and K6) were composed of black clay or
305 silty clay. Sediment cores from the Split Flat (K10, K11 and K12) were mainly black silt;
306 large quantity of shell fragments was found in the upper sections. Sediments in K10 were

307 grayish black, black and yellow deposits, suggesting complex material sources. The diversity
308 in the lithology decreased in the prodelta area (K2, K1, K9, and K8). Most of the sediments
309 here were black silt, and their surface layers had experienced disturbance by biomass.

310 The particle grain size of the core samples ranges from 4–6.5 φ, with significant vertical
311 variation (Fig. 7). The skewness, sorting coefficients and kurtosis for all core samples were
312 generally vertically homogeneous with small fluctuations. The core-averaged skewness
313 ranged from 0.05–0.4, and the kurtosis was close to 1 (from 0.83–1.25) in this area,
314 indicating an asymmetric logistic-normal distribution of the particle grain size in this region.
315 The sorting coefficients ranged from 1.36–2.13 φ, indicating particles were medium sorted.

316 # 4. Discussion

317 ## *4.1 Indication to the sedimentary environmental change in the YRE*

318 ### *4.1.1 Evidence from the age framework*

319 During sampling, PVC pipes at most sites reached a layer of yellow hard sand under the
320 sediments and could not be inserted any deeper. The maximum depth of seven cores, C3, K2,
321 K5, K6, K8, K11 and K12, corresponded to years around 1960. Accordingly, the hard sand
322 base in the estuary suggested there was an abnormal sedimentary event which altered the
323 deposition process around 1960. This layer of hard sand has the same components as the
324 subaqueous tidal ridges in the Western Korea Bay, which is the result of erosion from shoals
325 of the paleo-delta of the YRE during the Quaternary, when the sea level was low. Those
326 eroded materials from paleo-delta were then moved and deposited under the control of tidal

currents, and eventually formed the base of the geomorphology in the YRE (Cheng et al., 2012). Such changes can be tracked in cores with records before 1960s in this study:

Sediment cores C2, C5, K4, K10, K1 and K9 contain records before the 1960s. In the pre-1960 depositional phase of K4, the ^{137}Cs-derived sedimentation rate (calculated from Eqs. (3) and (4)) was significantly larger (1.92 cm/yr) than that after 1963 (0.94 cm/yr). Similar differences between pre- and post-1960s were also found in the ^{210}Pb-derived sedimentation rates of C2 and C5 in a previous study (Liu et al., 2017). Furthermore, the lithology of sediments deposited before 1963 in K4 differed significantly from those deposited after 1963 (Fig. 5). These results from K4, C2 and C5 imply that the rapid deposition process has likely been weakened after the 1960s near the Middle River.

The sedimentation rate in K10 (in the Split Flat area) before 1963 (2.91 cm/yr) was similar to that after 1963 (2.94 cm/yr), indicating that this site has had a continuous rapid deposition process during the last 60 years. In the prodelta area, the sedimentation rates in K1 and K9 before 1963 were both slightly smaller than after.

The ^{210}Pb curves for K1, K4, K9 and K10 all presented inverted sections before the 1960s, with larger concentrations at deeper layers. Such abnormal ^{210}Pb deposition before the 1960s was assumed to be caused by material mixing when “old” deposits with low ^{210}Pb activity eroded in adjacent areas in the estuary and were re-deposited at those sites (Andersen et al., 2000; Gao et al., 2017). This provides further evidence that the sedimentation process was different before the 1960s.

4.1.2 Evidence from grain size analysis

Although Liu et al. (2017) preliminarily discussed the potential relationship between occasional events and grain size change in cores C2, C3, C4 and C5, most results were based on single signal in one core thus may not represent the entirety of the environmental change. Thus, this section will further discuss the common pattern of long-term variation in particle grain size for the entire estuary using sediment cores collected in both 2013 and 2014 (Figs. 7 and 8). The grain size for 8 of 14 cores (C2, C3, C4, C5, K4, K5, K9 and K12) showed an overall decrease in mean particle grain size (an increase in φ) with depth after the 1960s, which indicates the particles were finer grained than in the past. The particles from four of the cores near the Split Flat and prodelta (K1, K2, K10 and K11) became coarser after 1963. The grain size in K6 and K8 did not show any obvious trend.

The mean grain size of cores near the Middle River (C2, C3, C4, C5, K4 and K5) and the two cores from other area (K9 and K12) became finer after the 1960s (Figs 7 and 8). This vertical variation of mean grain size near the Middle River was likely the result of human activity, specifically the construction of reservoirs in the river catchment. Due to the growth in population since the 1940s, 41 reservoirs were constructed in the watershed around the Yalu River; the largest reservoirs including the Yunfeng Reservoir were built up during the 1960s (Gao et al., 2012; Shi et al., 2017). In response to these constructions, the freshwater and sediment discharge of the river has experienced a decline over the last 50 years; this has been verified by monitoring data from the Huanggou Hydrology Station (Fig. 9). Compared to the first decade (1958 to 1967) with a total river discharge of $2.861 \times 10^{12} m^3$, the total river

368 discharge in a recent decade (1999 to 2008) was $1.93\times10^{12}m^3$, which decreased $9.31\times10^{11}m^3$
369 (32% of the former amount). Similarly, the total decadal sediment load decreased to 2.82×10^6
370 t during the decade from 1999 to 2008, which was only 17% of the amount in the first decade
371 (1.64×10^7 t). A recent study in Changjiang Estuary showed that the decrease in the sediment
372 load of the river resulted in downstream erosion that altered the deposition system (Gao et al.,
373 2019). Furthermore, the tidal action in the YRE was strengthened after 1960: the tidal range
374 at the estuarine entrance was 1.6 m in 1934–1943, but increased to 2.33 m after 1960 (Gao et
375 al., 2012).

376 The reduced fluvial sediment supply and the stronger tides have resulted in enhanced
377 erosion of the nearshore tidal flats. According to a previous study in the YRE (Gao et al.,
378 2012), the sea-bed sediments in the shallow water area outsidethe entrance line (where
379 massive tidal flats exist) are much finer than in the upstream river channel. Consequently, the
380 reduced sediment load from the river and the increased oceanic finer eroded materials
381 transported into the estuary by the stronger tides has led to a decreasing particle grain size
382 over time in sediment cores. The large quantity of coarse sediments trapped in the upstream
383 reservoirs constructed during the 1960s has further reduced the supply of coarse deposits to
384 the estuary. Thus, this anthropogenic influence on the sedimentation process has been
385 recorded in the mean grain size profiles, especially in cores near the Middle River (the main
386 water outlet).

4.2 ^{137}Cs sedimentary records under anthropogenic influence

4.2.1 Vertical variation in ^{137}Cs profiles

Figs. 2 and 10 demonstrate the vertical distributions of ^{137}Cs in the YRE; the major ^{137}Cs peaks ranged 1.36–7.39 Bq/kg, and secondary ^{137}Cs peaks ranged from 0.98–6.62 Bq/kg. There was at least one peak in the ^{137}Cs profile in all the core samples.

For cores C2, C3, C5, K2, K4, K6 and K10, the ^{137}Cs deposition curves before 1986 were mostly continuous or generally uninterrupted with the ^{137}Cs maximum peaks in each core corresponding to the 1963 ^{137}Cs time marker. The ^{137}Cs deposition curves in C2, C5, K4 and K10 were similar to the ideal atmospheric ^{137}Cs deposition curve (Figs. 2, 4 and 10). However, there was hiatus with long duration at multiple layers in ^{137}Cs profiles in C4, K1, K5, K8, K9, K11 and K12. Although ^{137}Cs was deposited discontinuously in K1, K5 and K8, the maximum ^{137}Cs peaks in these profiles still corresponded to the 1963 time marker, in accordance with the atmospheric deposition curve. The ^{137}Cs profiles in C4, K9, K11 and K12 differed from the atmospheric deposition curve: ^{137}Cs was found only at the surface layer in core C4, and the ^{137}Cs maximum peak in K12 was also near the surface; the maximum ^{137}Cs peaks in K9 and K11 were in the upper section (Figs. 2 and 10). The causes for these abnormal ^{137}Cs peaks are discussed in Section 4.2.2.

4.2.2 ^{137}Cs peaks without time markers

Most ^{137}Cs peaks in the profiles were considered as time markers. However, other ^{137}Cs peaks (which do not have corresponding time markers or match the ^{137}Cs ideal atmospheric

deposition curve) could signal changes in the sedimentation process. Although not every abnormal ^{137}Cs peak can be fully explained, the causes for most abnormal ^{137}Cs peaks can be identified. As the ^{137}Cs fallout started in 1954 and came to an end in 1986 with the cessation of atmospheric nuclear testing, these abnormal peaks were divided into two groups: pre-1986 and post-1986. The corresponding sediment layers were dated using Eqs. (3) and (4).

^{137}Cs deposition records before 1986 in the YRE

The three cores contained abnormal ^{137}Cs peaks for the period around 1980: K11 (dated to 1980); K8 (dated to 1981); and K2 (dated to 1982). There are two possible explanations for these peaks: (1) they could represent the 1986 auxiliary time marker considering their ages were close to 1986; (2) a significant environmental change happened in the Yalu River catchment at that time. Ran et al. (2012) showed the existence of such an environment change: the forest coverage around the lower reaches of the catchment decreased dramatically from 1.67×10^4 km^2 to 5.4×10^3 km^2 during the deforestation activity from 1958 to 1978. The subsequent increase in soil erosion probably provided more terrigenous sediment materials, which would to some extent explain the corresponding ^{137}Cs peaks the in sedimentary records (Iurian et al., 2012).

^{137}Cs deposition records after 1986 in the YRE

^{137}Cs activity after 1986 should have remained at low level in the YRE due to the absence of ^{137}Cs fallout (Fig. 4). However, several cores form the YRE contained marked ^{137}Cs contents after 1986.

Four cores contained ^{137}Cs peaks close to 1990: C3 (dated to 1992); K11 (dated to 1992); K10 (dated to 1991); and K1 (dated 1989). These cores were located near the East River, and the peaks might be related to large-scale mining activity in the lower reaches of catchment between the Middle and East River (north to the River Island). At the beginning of the 1990s, the mining volume was up to 3.8×10^5 t/yr, which was equivalent to 25% of the mean annual sediment load in the Yalu River basin (Ran et al., 2012). Open surface mining or dredging activity can induce resuspension of deposited materials and the older sediments could be exposed (Cundy et al., 2003), such process could lead to higher levels of radioactive concentration in coastal environments (Klubi et al., 2017), which may result in ^{137}Cs peaks in these cores.

Three cores contained ^{137}Cs peaks relating to years around 1995: K10 (dated to 1995); K1 (dated to 1997); and K9 (dated to 1997). The largest flood in the Yalu River drainage occurred in 1995. Such basin-wide flood usually leads to an extensive loss of surface soil, which is rich in ^{137}Cs; thus, ^{137}Cs peaks were formed in the estuarine sediments. However, this 1995 flood-induced ^{137}Cs can only be tracked in several cores in the estuary; as there may have been disturbances caused by physical and/or biological processes during the last 20 years from 1995.

There were also high ^{137}Cs levels in the surface sediments of cores C2, C3, C4, K2, K4, K5, K10 and K12 in the years after 2010, with peak values ranging from 0.19 to 0.72 Bq/kg. Core C4 had a very large sedimentation rate of 2.94 cm/yr according to dating results based on ^{210}Pb (Liu et al., 2017); Given the total length of this core, it only contained sediments

448 from the last 30 years, that is after 1986. There should have been no ^{137}Cs as there was no
449 more ^{137}Cs fallout after 1986. However, ^{137}Cs activity was observed at the surface layer in C4.
450 This core was collected in 2013 and the surface layer (top 4 cm) should be newly deposited
451 material from 2011 to 2013. However, the monthly sediment discharge in August 2012 at the
452 Huanggou Station was 1.7×10^5 t (4 times larger than that of August in normal year),
453 supplying plentiful terrigenous materials to the estuary. The surface ^{137}Cs in C4 was taken to
454 be a result of ^{137}Cs eroded from the surface soil eroded from the drainage and transported
455 by river flow. A similar explanation can be made for the surface peaks in C2 (dated to 2012),
456 C3 (dated to 2012) and K5 (dated to 2012). These sites were affected more by the river flow
457 as they were located near the Middle River (the main flow channel of the river), which
458 carried the bulk of the terrigenous sediment. Due to the gravity effect, eroded materials
459 carried by river upstream might be deposited near the lower reaches of the river and cannot
460 reach further south. Therefore, although C5 is also located near the Middle River, there was
461 no surface ^{137}Cs peak found in C5.

462 The reasons for the surface ^{137}Cs peaks in K10 (dated to 2004) and K12 (dated to 2007)
463 requires further study. A robust understanding of why the occasional environmental events
464 have different impacts at different sites also requires future studies using numerical
465 simulation.

466 5. Conclusion

467 This study provides an age framework for sedimentary records in the YRE using ^{210}Pb

468 dating results and verified by independent ^{137}Cs time markers. Decay curves in cores K4 and
469 K10 can be considered as the standard profiles for the sediment age framework in the study
470 area. The 1963 ^{137}Cs peak was recorded in most sediment cores in this area and was used as
471 the ideal key time marker, while 1954, 1975 and 1986 were considered as auxiliary time
472 markers.

473 The results show that the 1960s were a time when sedimentary environment in the YRE
474 experienced a dramatic change. Sediments deposited before 1960 could not be obtained at
475 most sites. Deposition near the Middle River after the 1960s was significantly slower than
476 before. In the 4 cores containing records before 1960, the ^{210}Pb activity behaved differently
477 before the 1960s than after, suggesting a change in the deposition process. The reduction of
478 coarse sediment supplies due to the reservoirs contributed to a decrease in the particle size of
479 deposits near the Middle River after 1963.

480 The vertical distribution of ^{137}Cs level showed a close relationship to sedimentary
481 environmental changes in the YRE. The ^{137}Cs peaks that were not time markers indicated that
482 sedimentation responses to both natural processes such as floods and human activity
483 including mining and deforestation in the basin.

484 This study is an example of understanding the impact of anthropogenic processes on
485 sedimentation in medium-scale estuaries. It also provides benchmarks for more robust coastal
486 management in coastal areas with increasing populations. In order to obtain further insight
487 into how different areas in the estuary respond differently to human interference, future
488 studies using numerical simulation are required.

Acknowledgments

This study was supported by the Natural Science Foundation of China (No. 41876087). We thank Liaodong University for providing the sediment core sample data. We also thank the staff of the Donggang Meteorological Station, the Donggang Oceanographic Station and the Huanggou Hydrological Station for supplying measurements on river discharges, tides, winds and wind waves in the study area. We are grateful to editorial help from Peter Mclntyre from UNSW Canberra. This is Publication No. 33 of the Sino-Australian Research Centre for Coastal Management.

References

Abril, J.M., 2016. A ^{210}Pb-based chronological model for recent sediments with random entries of mass and activities: Model development. J. Environ. Radioact. 151, 64–74. https://doi.org/10.1016/j.jenvrad.2015.09.018

Andersen, T.J., Mikkelsen, O.A., Annette, L.M., Pejrup, M., 2000. Deposition and mixing depths on some European intertidal mudflats based on Pb and Cs activities. Cont. Shelf Res. 20, 1569–1591.

Appleby, P.G., 1997. Sediment records of fallout radionuclides and their application to studies of sediment-water interactions. Water, Air Soil Pollut. 99, 573–585.

Cheng, Y., Liu, Y., Gao, J.H., Zhang, C.P., Li, F.X., Liu, J.W., Zhang, L., 2012. Influence of human activities on the riverbed evolution in Yalu River Estuary during recent one ventury. Acta Oceanol. Sin. 67, 609–620. (In Chinese with English abstract).

509 Cheng, Z., Wang, X., Paull, D., Gao, J., 2016. Application of the Geostationary Ocean Color
510 Imager to mapping the diurnal and seasonal variability of surface suspended matter in a
511 macro-tidal Estuary. Remote Sens. 8, 244–265. https://doi.org/10.3390/rs8030244
512 Collias, N.E., 1943. Statistical analysis of factors which make for success in initial encounters
513 between hens. Am. Nat. 77, 519–538.
514 Cundy, A.B., Croudace, I.W., Cearreta, A., Irabien, M.J., 2003. Reconstructing historical
515 trends in metal input in heavily-disturbed, contaminated estuaries: Studies from Bilbao,
516 Southampton Water and Sicily. Appl. Geochemistry 18, 311–325.
517 https://doi.org/10.1016/S0883-2927(02)00127-0
518 Folk, R.L., Ward, W.C., 1957. Brazos River bar: a study in the significance of grain size
519 parameters. J. Sediment. Res. 3–26.
520 Gao, J.H., Gao, S., Cheng, Y., Dong, L., Zhang, J., 2004. Formation of turbidity maxima in
521 the Yalu River Estuary, China. J. Coast. Res. 134–146.
522 Gao, J.H., Li, J., Wang, H., Bai, F. long, Cheng, Y., Wang, Y. ping, 2012. Rapid changes of
523 sediment dynamic processes in Yalu River Estuary under anthropogenic impacts. Int. J.
524 Sediment Res. 27, 37–49. https://doi.org/10.1016/S1001-6279(12)60014-6
525 Gao, J.H., Li, J., Wang Harry, V., Wang, Y., Wang, Z., Bai, F., Gao, S., Cheng, Y., 2009.
526 Distribution and their pollution assessment of heavy metals in the sediments of the Yalu
527 River Estuary and its adjacent coastal waters. Acta Oceanol. Sin. -English Ed. 28, 12–
528 23.
529 Gao, J.H., Jia, J., Sheng, H., Yu, R., Li, G.C., Wang, Y.P., Yang, Y., Zhao, Y., Li, J., Bai, F.,

530 Xie, W., Wang, A., Zou, X., Gao, S., 2017. Variations in the transport, distribution, and
531 budget of 210 Pb in sediment over the estuarine and inner shelf areas of the East China
532 Sea due to Changjiang catchment changes. J. Geophys. Res. Earth Surf. 122, 235–247.
533 https://doi.org/10.1002/2016JF004130
534 Gao, J.H., Shi, Y., Sheng, H., Kettner, A.J., Yang, Y., Jia, J.J., Wang, Y.P., Li, J., Chen, Y., Zou,
535 X., Gao, S., 2019. Rapid response of the Changjiang (Yangtze) River and East China
536 Sea source-to-sink conveying system to human induced catchment perturbations. Mar.
537 Geol. 414, 1–17. https://doi.org/10.1016/j.margeo.2019.05.003
538 Gwiazda, R., Paull, C.K., Ussler, W., Alexander, C.R., 2015. Evidence of modern
539 fine-grained sediment accumulation in the Monterey Fan from measurements of the
540 pesticide DDT and its metabolites. Mar. Geol. 363, 125–133.
541 https://doi.org/10.1016/j.margeo.2015.02.006
542 Humphries, M.S., Kindness, A., Ellery, W.N., Hughes, J.C., Benitez-Nelson, C.R., 2010.
543 ^{137}Cs and ^{210}Pb derived sediment accumulation rates and their role in the long-term
544 development of the Mkuze River floodplain, South Africa. Geomorphology 119, 88–96.
545 https://doi.org/10.1016/j.geomorph.2010.03.003
546 Iurian, A.-R., Begy, R., Cătinaş, I., Cosma, C., 2012. Results of medium-term soil
547 redistribution tates in Cluj County, Romania, using ^{137}Cs measurements. Procedia
548 Environ. Sci. 14, 22–31. https://doi.org/10.1016/j.proenv.2012.03.003
549 Japan Meteorological Agency, 2001. Bulletin of the Radioactivity (vo1． 83).
550 Jha, S.K., Chavan, S.B., Pandit, G.G., Sadasivan, S., 2003. Geochronology of Pb and Hg

551 pollution in a coastal marine environment using global fallout 137Cs. J. Environ.
552 Radioact. 69, 145–157. https://doi.org/10.1016/S0265-931X(03)00092-4
553 Jia, J., Yang, Y., Cai, T., Gao, J., Xia, X., Li, Y., Gao, S., 2018. On the sediment age estimated
554 by ^{210}Pb dating: probably misleading “prolonging” and multiple-factor-caused “loss.”
555 Acta Oceanol. Sin. 37, 30–39. https://doi.org/10.1007/s13131-018-1214-4
556 Kato, H., Onda, Y., Teramage, M., 2012. Depth distribution of ^{137}Cs, ^{134}Cs, and ^{131}I in soil
557 profile after Fukushima Dai-ichi Nuclear Power Plant Accident. J. Environ. Radioact.
558 111, 59–64. https://doi.org/10.1016/j.jenvrad.2011.10.003
559 Kirchner, G., 2011. 210Pb as a tool for establishing sediment chronologies: Examples of
560 potentials and limitations of conventional dating models. J. Environ. Radioact. 102,
561 490–494. https://doi.org/10.1016/j.jenvrad.2010.11.010
562 Klubi, E., Abril, J.M., Nyarko, E., Laissaoui, A., Benmansour, M., 2017. Radioecological
563 assessment and radiometric dating of sediment cores from dynamic sedimentary systems
564 of Pra and Volta estuaries (Ghana) along the Equatorial Atlantic. J. Environ. Radioact.
565 178–179, 116–126. https://doi.org/10.1016/j.jenvrad.2017.08.001
566 Koide, M., Soutar, A., Goldberg, E.D., 1972. Marine geochronology with ^{210}Pb. Earth Planet.
567 Sci. Lett. 14, 442–446. https://doi.org/10.1016/0012-821X(72)90146-X
568 Kumar, A., Hage-Hassan, J., Baskaran, M., Miller, C.J., Selegean, J.P., Creech, C.T., 2016.
569 Multiple sediment cores from reservoirs are needed to reconstruct recent watershed
570 changes from stable isotopes (δ^{13}C and δ^{15}N) and C/N ratios: case studies from the
571 mid-western United States. J. Paleolimnol. 56, 15–31.

572 https://doi.org/10.1007/s10933-016-9888-0

573 Leroy, S.A.G., Lahijani, H.A.K., Reyss, J.L., Chalié, F., Haghani, S., Shah-Hosseini, M.,
574 Shahkarami, S., Tudryn, A., Arpe, K., Habibi, P., Nasrollahzadeh, H.S., Makhlough, A.,
575 2013. A two-step expansion of the dinocyst Lingulodinium machaerophorum in the
576 Caspian Sea: The role of changing environment. Quat. Sci. Rev. 77, 31–45.
577 https://doi.org/10.1016/j.quascirev.2013.06.026

578 Li, L., Zhang, J., Ma, Y., Cui, X., 2012. Monitoring the coastline change in the Yalu River
579 Estuary from 1976 to 2010 based on remote sensing images. Bull. Surv. Mapp. 386–390
580 (In Chinese with English abstract).

581 Li, Y., Gao, S., 2012. Heavy metal characteristics in the sediment cores from Changjiang
582 subaqueous delta. Mar. Sci. Bull. 31, 154–161.

583 Li, Y., Li, A.C., Huang, P., Xu, F.J., Zheng, X.F., 2014. Clay minerals in surface sediment of
584 the north Yellow Sea and their implication to provenance and transportation. Cont. Shelf
585 Res. 90, 33–40. https://doi.org/10.1016/j.csr.2014.01.020

586 Ligero, R.A., Barrera, M., Casas-Ruiz, M., 2005. Levels of ^{137}Cs in muddy sediments of the
587 seabed of the Bay of Cádiz, Spain. Part I. Vertical and spatial distribution of activities. J.
588 Environ. Radioact. 80, 75–86. https://doi.org/10.1016/j.jenvrad.2004.05.019

589 Liu, Y., Cheng, Y., Gao, J.H., Zheng, J.H., Zhang, C.P., Zhang, L., Liu, J.W., 2017. The
590 coupling of the sedimentary records in the Yalu River estuary and the adjacent western
591 coasts. Acta Oceanol. Sin. 39, 76–88.
592 https://doi.org/10.3969/j.issn.0253-4193.2017.01.008. (In Chinese with English

593 abstract).

594 Liu, Y., Cheng, Y., Li, H., Liu, J., Zhang, C., Zhang, L., Zheng, C., Gao, J., 2013. Provenance
595 tracing of indicative minerals in sediments of the Yalu River Estuary and its adjacent
596 shallow seas. J. Coast. Res. 290, 1227–1235.
597 https://doi.org/10.2112/JCOASTRES-D-12-00269.1

598 Martins, V., Figueira, R.C.L., França, E.J., Ferreira, P.A. de L., Martins, P., Santos, J.F., Dias,
599 J.A., Laut, L.L.M., Monge Soares, A.M., Silva, E.F. da, Rocha, F., 2012. Sedimentary
600 processes on the NW Iberian Continental Shelf since the Little Ice Age. Estuar. Coast.
601 Shelf Sci. 102–103, 48–59. https://doi.org/10.1016/j.ecss.2012.03.004

602 Mulsow, S., Piovano, E., Cordoba, F., 2009. Recent aquatic ecosystem response to
603 environmental events revealed from ^{210}Pb sediment profiles. Mar. Pollut. Bull. 59, 175–
604 181. https://doi.org/10.1016/j.marpolbul.2009.05.018

605 Pálsson, S.E., Howard, B.J., Wright, S.M., 2006. Prediction of spatial variation in global
606 fallout of ^{137}Cs using precipitation. Sci. Total Environ. 367, 745–756.
607 https://doi.org/10.1016/j.scitotenv.2006.01.011

608 Poręba, G.J., Bluszcz, A., 2007. Determination of the initial ^{137}Cs fallout on the areas
609 contaminated by chernobyl fallout. Geochronometria 26, 35–38.
610 https://doi.org/10.2478/v10003-007-0009-y

611 Prajith, A., Rao, V.P., Chakraborty, P., 2016. Distribution, provenance and early diagenesis of
612 major and trace metals in sediment cores from the Mandovi estuary, western India.
613 Estuar. Coast. Shelf Sci. 170, 173–185. https://doi.org/10.1016/j.ecss.2016.01.014

614 Qiao, S., Shi, X., Wang, G., Zhou, L., Hu, B., Hu, L., Yang, G., Liu, Y., Yao, Z., Liu, S., 2017.
615 Sediment accumulation and budget in the Bohai Sea, Yellow Sea and East China Sea.
616 Mar. Geol. 390, 270–281. https://doi.org/10.1016/j.margeo.2017.06.004
617 Ran, L., Shi, Y., Gao, J., Liu, Y., Li, F., Bai, F., Li, J., 2012. Gain size variation and its
618 influencing factors in the sediment cores of west flat in Yalu River Estuary. Mar. Geol.
619 Quat. Geol. 32, 31–42. https://doi.org/10.3724/sp.j.1140.2012.02031. (In Chinese with
620 English abstract).
621 Ritchie, J.C., McHenry, J.R., 1990. Application of Radioactive Fallout Cesium-137 for
622 Measuring Soil Erosion and Sediment Accumulation Rates and Patterns: A Review. J.
623 Environ. Qual. 19, 215. https://doi.org/10.2134/jeq1990.00472425001900020006x
624 Ruiz-Fernández, A.C., Hillaire-Marcel, C., 2009. ^{210}Pb-derived ages for the reconstruction of
625 terrestrial contaminant history into the Mexican Pacific coast: Potential and limitations.
626 Mar. Pollut. Bull. 59, 134–145. https://doi.org/10.1016/j.marpolbul.2009.05.006
627 Ruiz-Fernández, A.C., Páez-Osuna, F., Urrutia-Fucugauchi, J., Preda, M., 2005. ^{210}Pb
628 geochronology of sediment accumulation rates in Mexico City Metropolitan Zone as
629 recorded at Espejo de los Lirios lake sediments. Catena 61, 31–48.
630 https://doi.org/10.1016/j.catena.2005.01.003
631 Shi, Y., Gao, J.H., Sheng, H., Du, J., Jia, J.J., Wang, Y.P., Li, J., Bai, F.L., Chen, Y.N., 2018.
632 Cross-front sediment transport induced by quick oscillation of the Yellow Sea Warm
633 Current: Evidence from the sedimentary record. Geophys. Res. Lett. 1–9.
634 https://doi.org/10.1029/2018GL080751

635 Shi, Y., Liu, Z., Gao, J., Yang, Y., Wang, Y., 2017. The response of sedimentary record to
636 catchment changes induced by human activities in the western intertidal flat of Yalu
637 River Estuary, China. Acta Oceanol. Sin. 36, 54–63.
638 https://doi.org/10.1007/s13131-016-0941-7
639 Simms, A.D., Woodroffe, C., Jones, B.G., Heijnis, H., Mann, R.A., Harrison, J., 2008. Use of
640 ^{210}Pb and ^{137}Cs to simultaneously constrain ages and sources of post-dam sediments in
641 the Cordeaux reservoir, Sydney, Australia. J. Environ. Radioact. 99, 1111–1120.
642 https://doi.org/10.1016/j.jenvrad.2008.01.002
643 Szmytkiewicz, A., Zalewska, T., 2014. Sediment deposition and accumulation rates
644 determined by sediment trap and ^{210}Pb isotope methods in the Outer Puck Bay (Baltic
645 Sea). Oceanologia 56, 85–106. https://doi.org/10.5697/oc.56-1.085
646 Tsabaris, C., Patiris, D.L., Fillis-Tsirakis, E., Kapsimalis, V., Pilakouta, M., Pappa, F.K.,
647 Vlastou, R., 2015. Vertical distribution of ^{137}Cs activity concentration in marine
648 sediments at Amvrakikos Gulf, western of Greece. J. Environ. Radioact. 144, 1–8.
649 https://doi.org/10.1016/j.jenvrad.2015.02.009
650 Tsurumura, T., Tsumori, Y., Qiu, H., Oda, M., Sakurai, J., Nagahama, M., Tsuge, H., 2013.
651 Arginine ADP-ribosylation mechanism based on structural snapshots of iota-toxin and
652 actin complex. Proc. Natl. Acad. Sci. 110, 4267–4272.
653 https://doi.org/10.1073/pnas.1217227110
654 Varley, A., Tyler, A., Dowdall, M., Bondar, Y., Zabrotski, V., 2017. An in situ method for the
655 high resolution mapping of ^{137}Cs and estimation of vertical depth penetration in a highly

contaminated environment. Sci. Total Environ. 605–606, 957–966. https://doi.org/10.1016/j.scitotenv.2017.06.067

Wang, X.H., Wang, D.P., Sun, Z., He, Z., Liu, H., Guan, W., Chen, D., Ding, P., He, Q., Wang, H., Bao, X., Gan, J., Geyer, W.R., Li, L., Liu, J.T., Lowe, R., Winterwerp, J.C., Wolanski, E., Yin, K., You, Z.J., Zhu, J., 2016. International scientists discuss impact on China's estuarine and coastal environment by intensive anthropogenic activities - The 2nd workshop on sediment dynamics of muddy coasts and estuaries: Physics, biology and their interactions, Zhoushan, China. Estuar. Coast. Shelf Sci. 23–168, ii–iii. https://doi.org/10.1016/S0272-7714(15)00342-X

Wang, Z.H., Dong, Y.H., Chen, J., Li, X.F., Cao, J., Deng, Z.Y., 2014. Dating recent sediments from the subaqueous Yangtze delta and adjacent continental shelf , China The lacustrine hybrid sedimentary environment in Jurassic Sichuan Basin and its reservoir character. J. Palaeogeogr. 3, 207–218. https://doi.org/10.3724/SP.J.1261.2014.00052

Yu, Q., Wang, Y., Gao, J., Gao, S., Flemming, B., 2014. Turbidity maximum formation in a well-mixed macrotidal estuary: The role of tidal pumping. J. Geophys. Res. Ocean. 119, 7705–7724. https://doi.org/10.1002/2014JC010228

List of Tables

Table 1 ^{210}Pb-derived and ^{137}Cs-derived sedimentation rates and chronological framework in the YRE. "*" denotes published results from Liu (Liu et al., 2017).

Area	Core Number	^{210}Pb Decay Section	^{210}Pb-derived Sedimentation Rate (cm/yr)	^{137}Cs Primary Time Marker	^{137}Cs Auxiliary Time Markers	^{137}Cs-derived Sedimentation Rate (cm/yr)
River Island	K4	0-60cm	1.33	1963 (48cm)	1975 (38cm)	0.94
	K5	6-30cm	1.13	1963 (67cm)	-	1.31
		38-63cm	1.09			
	K6	-	-	1963 (104cm)	-	2.04
Split Flat	K10	54-136cm	2.24	1963 (148cm)	1954 (172cm)	2.90
	K11	-	-	1963 (82cm)	-	1.61
	K12	26-92cm	1.80	1963 (96cm)	-	1.88
Prodelta	K1	14-70cm	1.80	1963 (82cm)	1986 (40cm)	1.61
	K2	0-44cm	1.36	1963 (98cm)	1975 (80cm)	1.92
	K8	26-74cm	2.83	1963 (104cm)	-	2.04
	K9	8-74cm	1.77	1963 (80cm)	-	1.57
Middle River	C2*	-	-	1963 (132cm)	1954 (156cm)	2.64
					1975 (104cm)	
					1986 (72cm)	
	C3*	0-32cm	1.04	1963 (72cm)	1986 (40cm)	1.44
	C4*	8-70cm	2.94	-	-	-
	C5*	8-50cm	1.54	1963 (74cm)	1954 (98cm)	1.48
		110-132cm	1.48		1986 (44cm)	

677

678 **List of Figures**

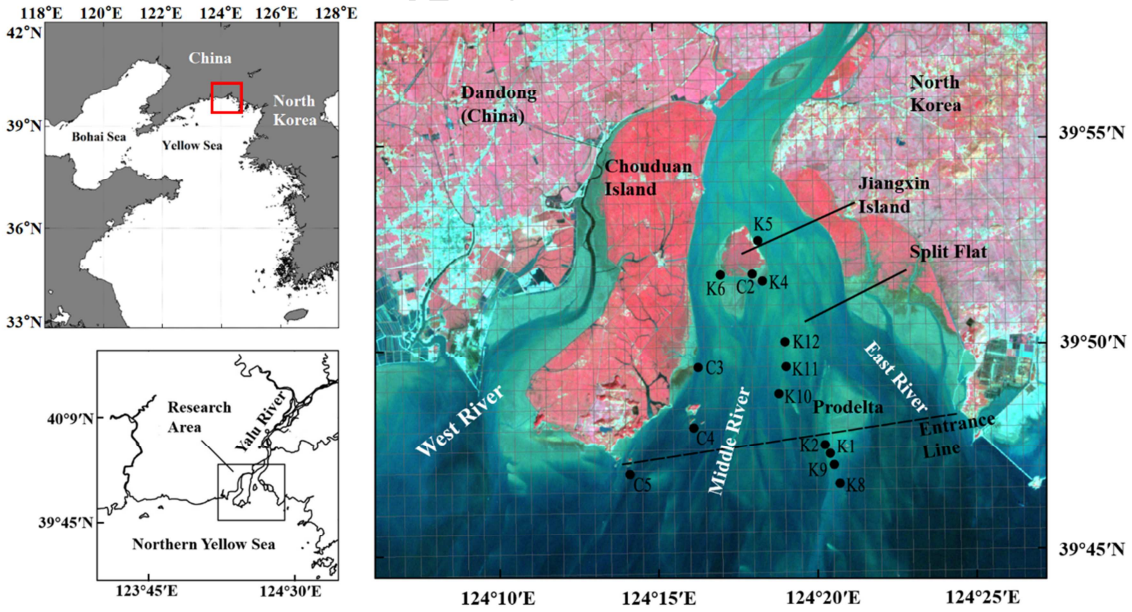

679

680 **Figure. 1** Locations of sampling sites. K1, K2, K4, K5, K6, K8, K9, K10, K11 and K12

represent samples in this study while C2, C3, C4 and C5 are samples published in Liu (Liu et al., 2017). K4, K5 and K6 denote sampling sites near the River Island; Sites K12, K11, and K10 are near the Split Flat between the Middle River and East River; K1, K2, K8 and K9 are sampling sites from the prodelta area outside the estuary entrance; C2, C3, C4 and C5 represent sampling sites along the Middle River.

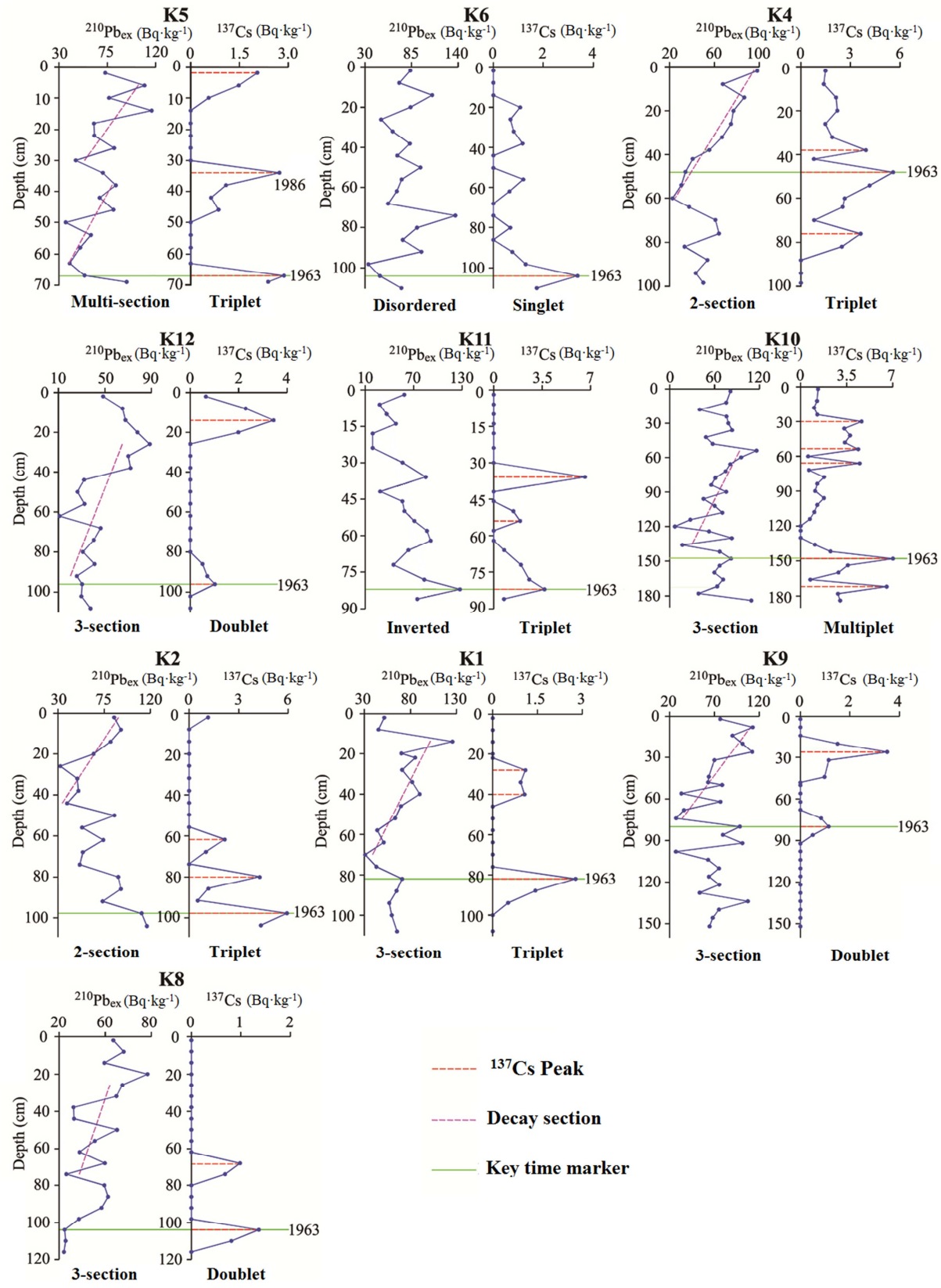

687

688 **Figure. 2** Vertical profiles of ^{210}Pb and ^{137}Cs from 10 sediment cores. The ^{210}Pb decay curves

689 were classified into five types based on the curve patterns. The ^{137}Cs profiles were classified

690 into four types based on the numbers of ^{137}Cs peaks.

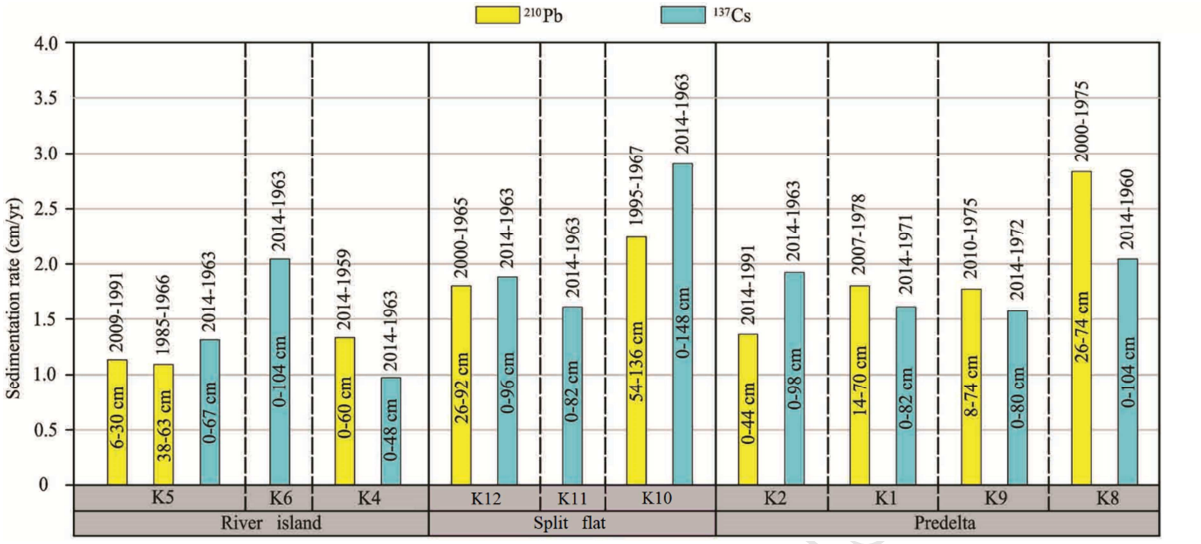

691

692 **Figure. 3** Comparison of sedimentation rates based on the ^{210}Pb decay curves and ^{137}Cs time

693 markers. Core K5 contained two ^{210}Pb decay sections. Cores K6 and K11 contained no ^{210}Pb

694 decay section. Sectioned sedimentation rates for core K4 were calculated based on the 1975

695 and 1963 time markers.

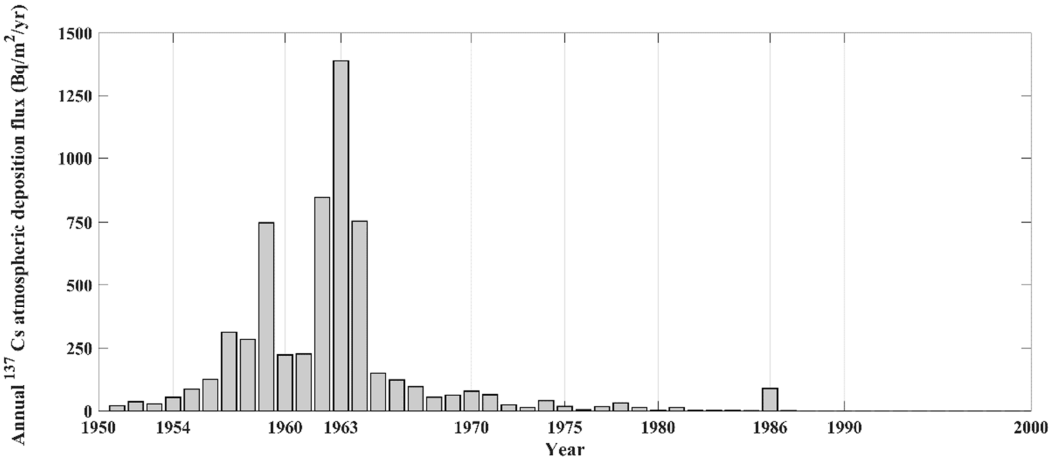

696

697 **Figure. 4** Estimated annual ^{137}Cs atmospheric deposition flux in the YRE.

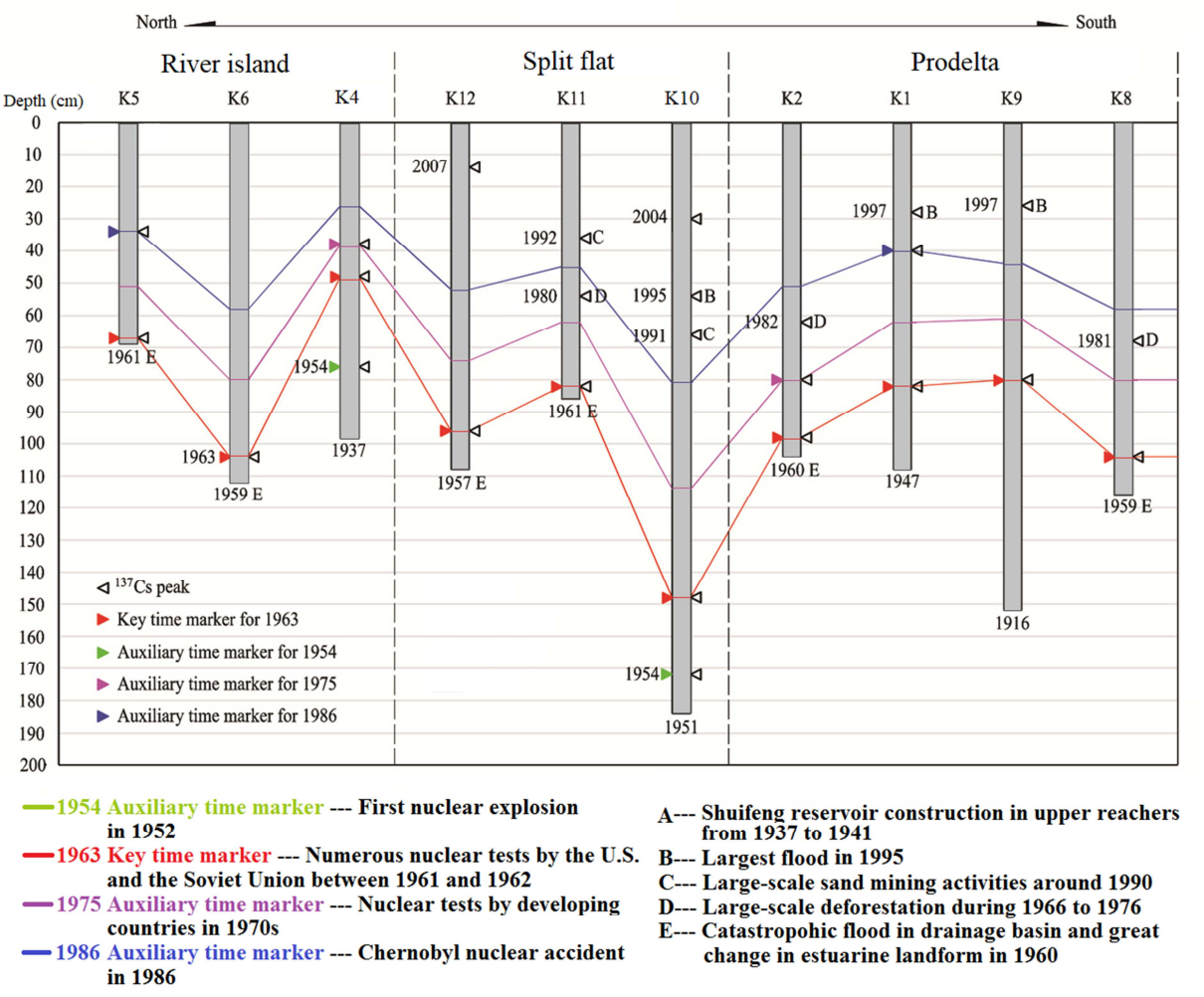

Figure. 5 Sedimentation ages and time markers in the YRE and sedimentary events in the river basin. The 1963 time marker appeared in all 10 cores of the YRE. The 1954, 1975, and 1986 time markers appeared once, twice, and twice, respectively. Some ^{137}Cs peaks corresponded to sedimentary events, and the differences in sedimentary rates among different depositional areas were based on the spacing distance of age lines, as well as on the relationships between lithological characteristics and sedimentary ages in different depositional areas.

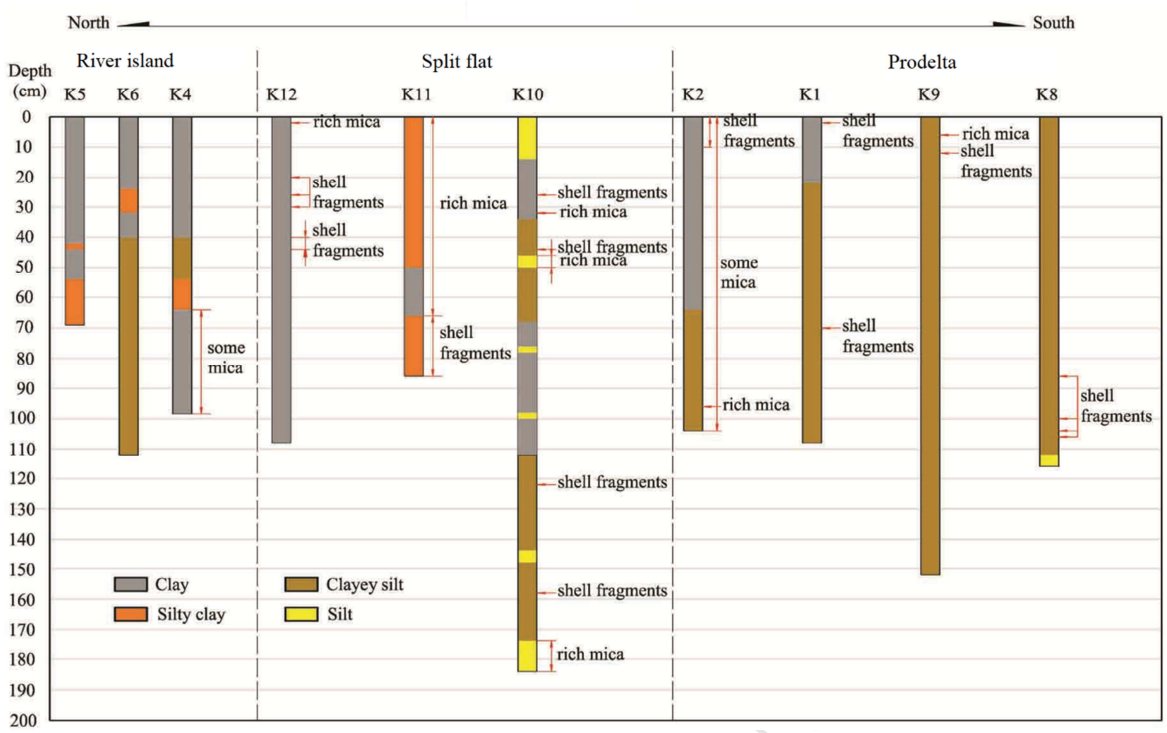

706

707 **Figure. 6** Lithological characteristics of sediment cores collected in 2014.

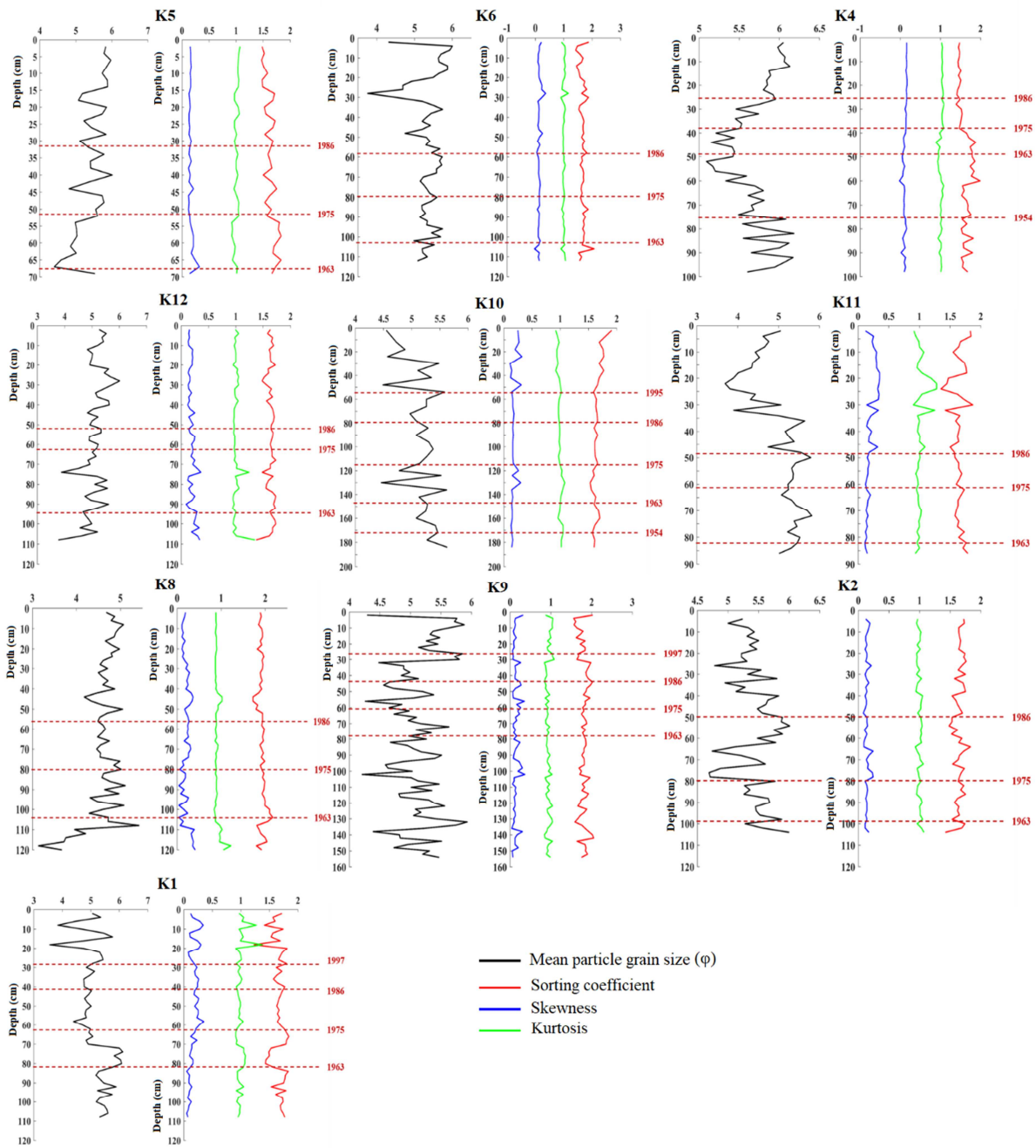

Figure. 7 Grain size analysis of cores collected in 2014. Black lines represent mean particle grain size (φ). Blue, green and red lines denote the skewness, kurtosis and sorting coefficient, respectively.

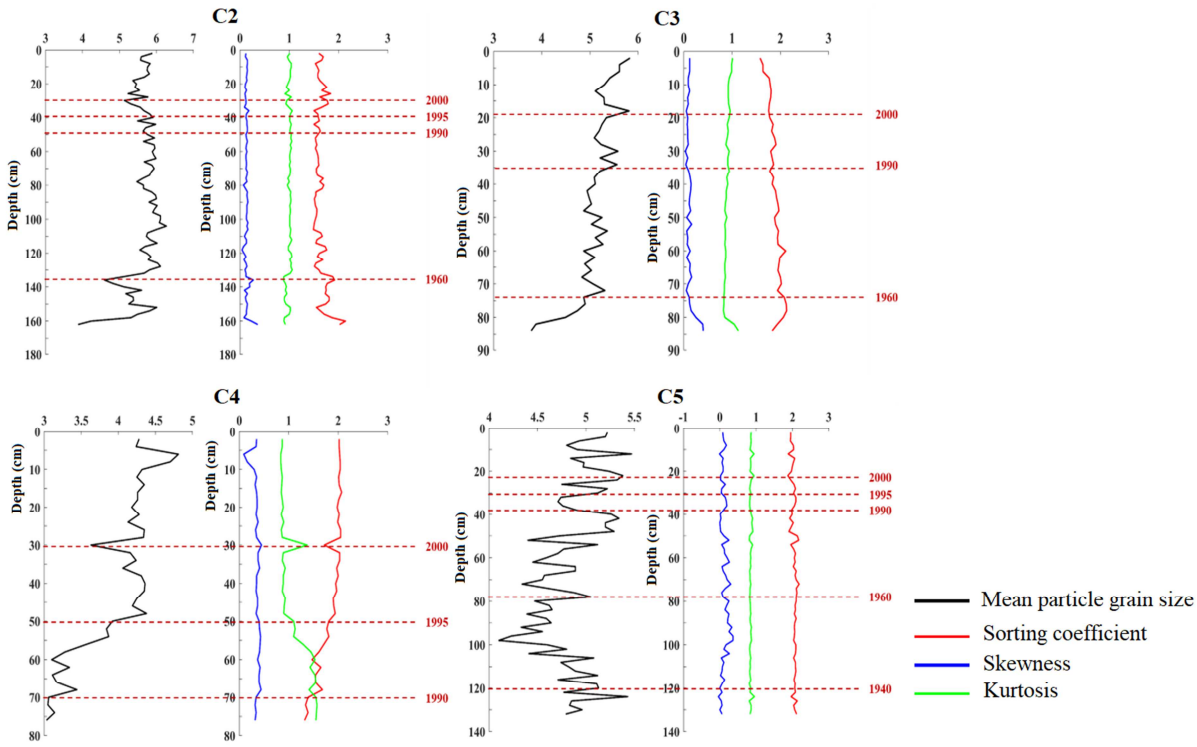

712

713 **Figure. 8** Grain size analysis of cores (modified from (Liu et al., 2017)). Black lines

714 represent mean particle grain size (φ). Blue, green and red lines denote the skewness, kurtosis

715 and sorting coefficient, respectively.

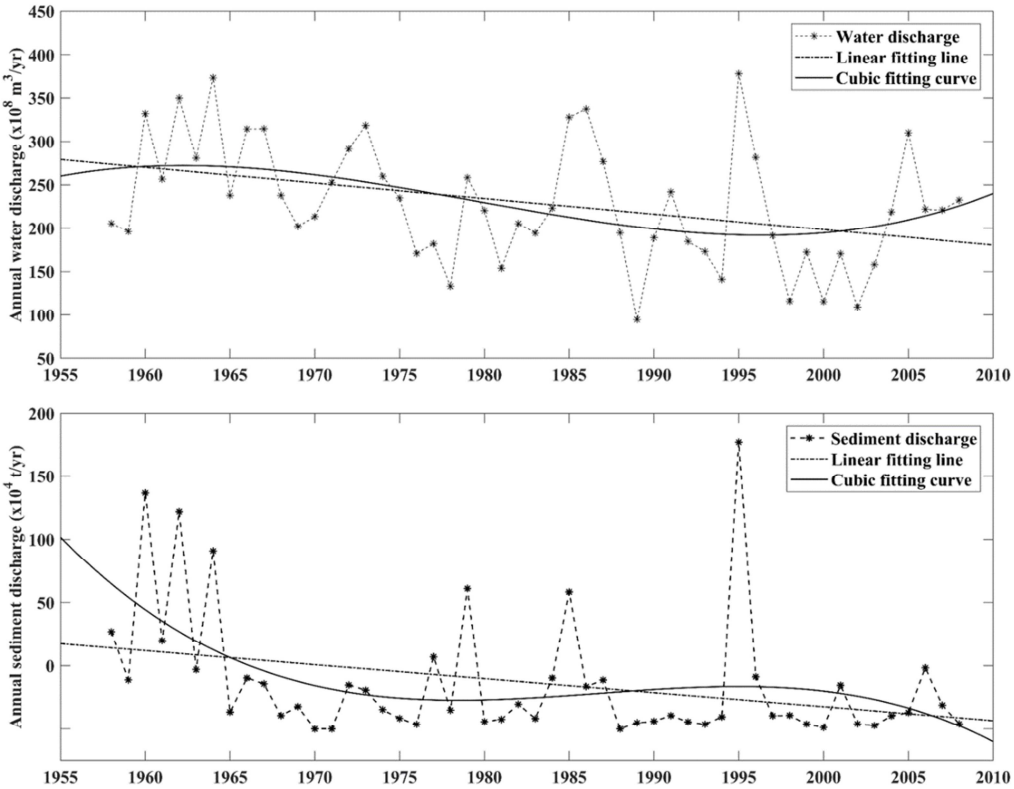

716

717 **Figure. 9** Annual freshwater discharge and sediment load at Huanggou Hydrology Station

718 from 1958 to 2008.

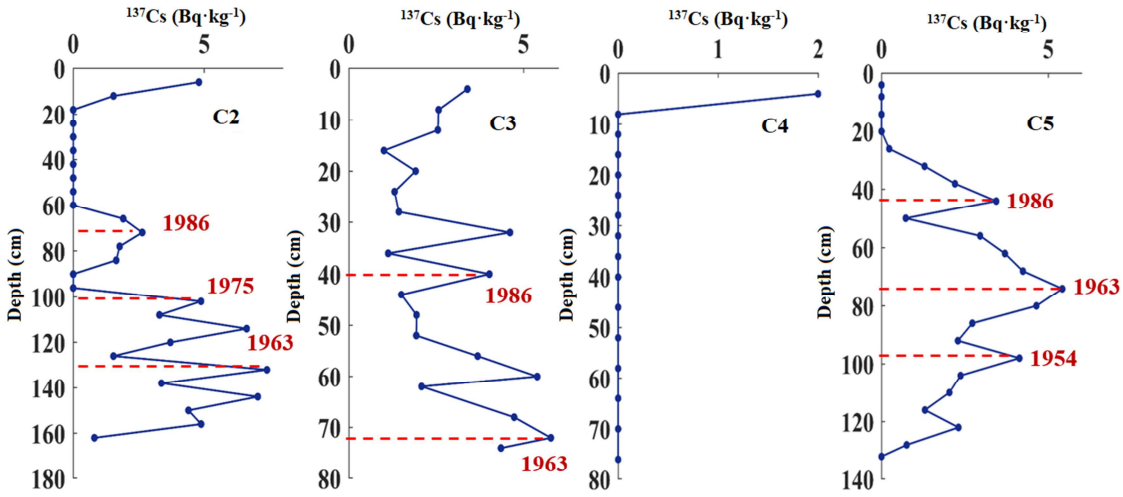

719

720 **Figure. 10** ^{137}Cs profiles of C2, C3, C4 and C5.

721